Transport in Porous Media **12:** 125–141, 1993.

A Geometrical Model for Numerical Simulation of Capillary Imbibition in Sedimentary Rocks

CLAUDE HAMMECKER, JEAN-DIDIER MERTZ, CHRISTIAN FISCHER, and DANIEL JEANNETTE
Centre de Géochimie de la Surface (C.N.R.S.), 67084 Strasbourg Cedex, France

(Received: 25 September 1991; in final form: 28 January 1992)

Abstract. The cylindrical model is discussed and a new tube model is proposed to describe capillary imbibition kinetics in porous sedimentary rocks. The tube consists of a periodic succession of a single hollow spherical element of which the geometry is defined by the sphere radius and the sphere access radius. These two parameters are estimated experimentally for four rock types from their specific surface areas. Introducing those parameters in the model capillary imbibition kinetics, parameters are calculated and compared with the experimental ones. A direct relation between imbibition kinetics and specific surface area has been pointed out.

Key words. Capillary imbibition kinetics, tube model, spherical pore shape, numerical simulation, sedimentary rocks, specific surface area, surface roughness.

1. Introduction

By studying, experimental capillary imbibition of water in porous sedimentary rocks, two quantitative kinetic parameters can be measured (the capillary rise and the amount of absorbed water rates). As their values are representative of the porous network geometry, it is interesting to quantify this relation and to predict these parameters from experimental pore structures and dimensions.

On the basis of the Washburn law (1921), the capillary imbibition phenomenon has been simulated by many cylindrical or conical models (Szekely *et al.*, 1971; Dullien 1979; Levine *et al.*, 1980). Although these models describe the capillary behaviour of natural rocks, the dimensions (pore radii) of the simulated porous networks are incompatible with the real geometry.

Despite the complex structure of natural porous media, like sedimentary rocks, a simple geometric model according to experimental dimension data (microscopical observation, mercury porosimetry, BET surface area) is elaborated. A numerical simulation of capillary imbibition in the proposed model is tested for various clayless sedimentary rocks: Laspra dolomitic limestone, Hontoria limestone, Lourdines limestone and Fontainebleau sandstone. The experimental values of the free porosity (N_l), the average pore radius (R) and the average pore access radius (r_1) for each rock, make it possible to calculate the two capillary kinetic parameters.

2. Experiment

The capillary imbibition kinetic measurement is usually performed with cylindrical core samples of 3.5 or 4 cm diameter and about 7 cm high (Dullien *et al.*, 1977; Bousquie, 1979; Mertz, 1989). They are previously dried in an oven at 60°C, until constant weight is reached. Then they are cooled at 20°C in a closed container in presence of silica gel maintaining a dry atmosphere. Afterwards they are placed vertically on a thick wet filter paper providing a regular and continuous water supply. This set is tightly enclosed in a methacrylate container in order to maintain a vapour saturated atmosphere and to avoid the superposition of any evaporation process during the experiment. At regular increasing time intervals, the weight of the rock samples and the height of the wetted fringe observable on the surface of each one, are measured. The results are plotted as an amount of absorbed water increase $\Delta W/S$ (cm^3 of water/cm^2 of column area) and/or height of capillary rise Δl (cm) versus the square root of time $\sqrt{t}$ (Figure 1). A typical feature of capillary imbibition in rocks is the linear evolution with the square root of time of these two parameters, at least in the first stage of the experiment. Capillary rise rate and weight increase are linear until water reaches the top of the sample. Nevertheless, after this first stage, which is unique for height of capillary rise, weight increase proceeds but drastically slows down. The first stage corresponds to the saturation of the free accessible porous network (N_l) by a genuine capillary imbibition mechanism which fills 70 to 85% of the total pore space whereas the second one coincides with a diffusion process where trapped air bubbles dissolve into water (Mertz, 1989). As the purpose of this work is the exclusive study of capillary kinetics, the second stage of weight increase will not be examined. In order to quantify capillary imbibition kinetics, the

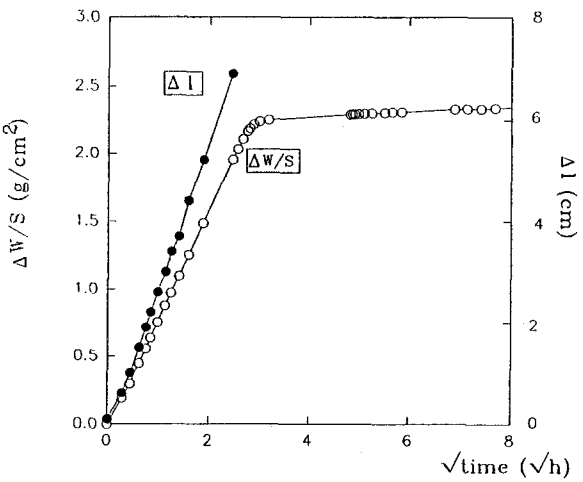

Fig. 1. Experimental capillary imbibition kinetic height of capillary rise (Δl) and amount of absorbed water ($\Delta W/S$) versus square root of time ($\sqrt{t}$).

slopes of those first stage straight lines are measured. Two characteristic kinetic parameters are defined:

$$A = \Delta W/(S\sqrt{t}) \quad \text{and} \quad B = \Delta l/(\sqrt{t}).$$

Attention must be paid to the fact that this perfect linear evolution of weight increase and height of capillary rise, with the square root of time, occurs only in homogeneous and well sorted rocks, which lack sharp stratification planes and clay minerals. In this type of rock, weight increase and height of capillary rise progress simultaneously, and the A/B rate is equal or similar to the free porosity value (N_1): $N_l \approx A/B$. As this criterion is generally verified, especially in homogeneous rocks, the following model of capillary imbibition simulation, considers height of capillary rise kinetic (B) only.

3. The Cylindrical Model

The cylindrical element is the simplest pore shape for the mathematical formulation of capillary imbibition phenomenon in porous bodies. Fluid flow (Q) through a cylindrical tube is directly expressed as a function of fluid viscosity ($\eta = 1.019 \times 10^{-3}$ PI for water), pressure gradient (ΔP) and tube dimensions (radius r and length l) in the Hagen–Poiseuille formula:

$$Q = \frac{\pi r^2 \, \mathrm{d}l}{\mathrm{d}t} = \frac{\pi r^4 \Delta P}{8\eta l}. \tag{1}$$

For a quasi-steady-state capillary imbibition into a cylindrical tube while neglecting the gravity action, the pressure gradient is given by the Laplace equation:

$$\Delta P = P_c = \frac{2\gamma \cos\theta}{r}, \tag{2}$$

where γ is surface tension of water (0.072 N m^{-1}), θ is the contact angle (in general to be considered 0) and r the capillary radius.

Combining both formulae, Washburn (1921) related capillary imbibition kinetic with fluid properties and capillary dimensions:

$$\frac{\mathrm{d}l}{\mathrm{d}t} = \frac{r\gamma}{4\eta l} \Rightarrow l = \sqrt{\frac{r\gamma}{2\eta}}t + l_0^2. \tag{3}$$

When $l_0 = 0$ for $t = 0$, rising damp migration and weight increase kinetics can be formulated as simple square root functions:

$$l = B\sqrt{t}, \qquad v = A\sqrt{t} \tag{4}$$

where

$$B = \sqrt{(r\gamma/2\eta)} \quad \text{and} \quad A = \rho\pi r^2\sqrt{(r\gamma/2\eta)}.$$

The pattern of this expression is similar to experimental observation of the capillary imbibition kinetics (Figure 1). However using this formula to calculate the average radius of a rock sample, knowing the experimental values of A and B, does not give realistic results (Mertz, 1989). The radii calculated with this formula are considerably smaller than realistic for sedimentary rocks: a 10^3 to 10^4 factor relates the measured pore radii by microscopical observation and the calculated ones (Figure 2). Even by introducing the gravity influence, acting as an adverse force to capillary rise of water, the results would not vary enough to reach more realistic values, because the gravity action is almost negligible in comparison with so high capillary pressures (due to the excessively small size of calculated capillaries). Although this model describes the shape of experimental capillary imbibition curves, it is not satisfactory because of its lack of agreement with real pore sizes and structures.

4. The Spherical Model

By working with geometrical networks built with cylindrical or conical elements periodically repeated, or by dealing with sinusoidal capillary profiles, Kusakov and Nekrasov (1966), Van Brakel (1975), Dullien *et al.* (1977), Levine *et al.* (1980), and Marmur (1989), show the evidence of capillary pressure modifications, generated by the meniscus radius variations during the imbibition process. On the basis of this kind of work and in order to get coherent pore dimensions agreeing with experimental pore size and rate of capillary rise data of porous sedimentary rocks, we used a model of tube, built with a periodically repeated sphere shape. Despite its poor agreement with genuine pore structure, the spherical pore shape was chosen for its simple geometry and therefore its easy mathematical formulation.

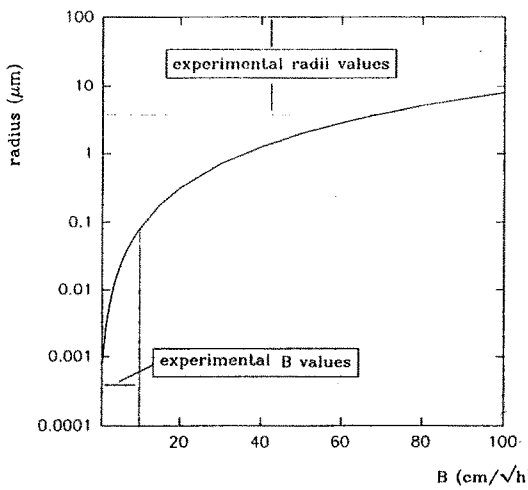

Fig. 2. Variation of capillary radii versus B for cylindrical model.

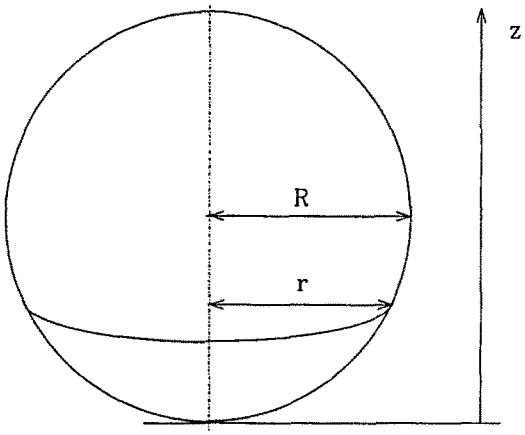

Fig. 3. Meniscus radius variation in sphere.

In the case of a vertical capillary rise of water into a sphere, the meniscus suffers a continuous variation of its radius along the z axis (Figure 3). The meniscus radius r can be expressed as a function of height z in the sphere as:

$$r(z) = (2Rz - z^2)^{1/2},$$

where R is the sphere radius.

Consequently the capillary pressure also varies during the imbibition and becomes a z-function:

$$\Delta P = \frac{2\gamma}{r(z)} = \frac{2\gamma}{(2Rz - z^2)^{1/2}}.$$

Gravity has to be considered as an adverse force limiting the force giving rise to water. The total pressure gradient is the difference between capillary pressure and the water column's weight, and can be expressed as:

$$\Delta P = \frac{2\gamma}{r(z)} - \rho g z, \tag{5}$$

where ρ is water density (1 g cm^{-3}), g the gravitational constant (9.8066 m s^{-2}), and z the water height upon the free water surface. On the other hand, as the flow through a hollow system only depends on the smallest section of the fluid path, it will depend on access orifice radius r_1. Despite the Hagen-Poiseuille equation being defined for cylindrical tubes, it can be applied considering a quasi steady-state imbibition into a spherical element, which can be seen as stack of infinite thin cylindrical sections. This equation is then formulated with this new capillary pressure expression:

$$Q = \frac{\pi r_1^4}{8\eta z}\left(\frac{2\gamma}{r(z)} - \rho g z\right), \tag{6}$$

$$\frac{\pi r(z)^2\,\mathrm{d}z}{\mathrm{d}t} = \frac{\pi r_1^4}{8\eta z}\left(\frac{2\gamma}{r(z)} - \rho g z\right),$$

$$\frac{\mathrm{d}z}{\mathrm{d}t} = \frac{r_1^4}{8\eta z r(z)^2}\left(\frac{2\gamma}{r(z)} - \rho g z\right). \tag{7}$$

Equation (7) describes the instantaneous velocity of capillary imbibition in a spherical element as a function of z. When imbibition velocity $\mathrm{d}z/\mathrm{d}t$ is plotted versus height z (Figure 4a), for a constant sphere radius R (100 μm in this case), various conclusions can be drawn:

- $\mathrm{d}z/\mathrm{d}t$ increases at both ends of the sphere, as $r(z)$ decreases, but this equation is indeterminate ($\mathrm{d}z/\mathrm{d}t \to \infty$) when $r(z)$ tends to zero;
- the access orifice radius r_1 performs a decisive role in imbibition velocity ($\mathrm{d}z/\mathrm{d}t$);
- the lowest velocity occurs for higher z value than sphere equator ($z = R$);
- average imbibition velocity decreases regularly for the following spherical elements (Figure 4b).

The indetermination of this equation can be resolved, considering the limits where both access orifices cut the spherical element, reducing the liquid path from $2R$ to $\varepsilon_2 - \varepsilon_1$ (Figure 5) where

$$\varepsilon_1 = R - (R^2 - r_1^2)^{1/2}, \qquad \varepsilon_2 = R + (R^2 - r_1^2)^{1/2}.$$

So imbibition velocity $\mathrm{d}z/\mathrm{d}t$ has a finite maximal value when the meniscus reaches the sphere limits. Further, in order to get an expression of the cumulative imbibition time as a function of the total height, Equation (7) becomes

$$\mathrm{d}t = \frac{8\eta z r(z)^3\,\mathrm{d}z}{r_1^4(2\gamma - r(z)\rho g z)}. \tag{8}$$

To avoid the complicated analytical integration of this equation, it has been solved numerically with computer iterations, using a small $\mathrm{d}z$ incremental value: $\mathrm{d}z = (\varepsilon_2 - \varepsilon_1)/1000$. Hence for each $\mathrm{d}z$ increment, z, $\mathrm{d}t$ and t are recalculated as

$$z = \sum_{\varepsilon_1}^{\varepsilon_2} \mathrm{d}z \quad \text{and} \quad t = \sum \mathrm{d}t(z).$$

The numerical integration provides the capillary imbibition kinetics into a single spherical element (Figure 6a). As may be expected the result does not agree with a square root function. Nevertheless, considering a tube with a length of several centimetres (L) built with a large number (n) of spherical elements ($L = \Sigma_{j=1}^{n}(\varepsilon_2 - \varepsilon_1)$), Equation (8) becomes

$$\mathrm{d}t = \frac{8\eta(\Sigma(\varepsilon_2 - \varepsilon_1)_{j-1} + z_j) r(z_j)^3\,\mathrm{d}z}{r_1^4(2\gamma - r(z_j)\rho g(\Sigma(\varepsilon_2 - \varepsilon_1)_{j-1} + z_j)} \tag{9}$$

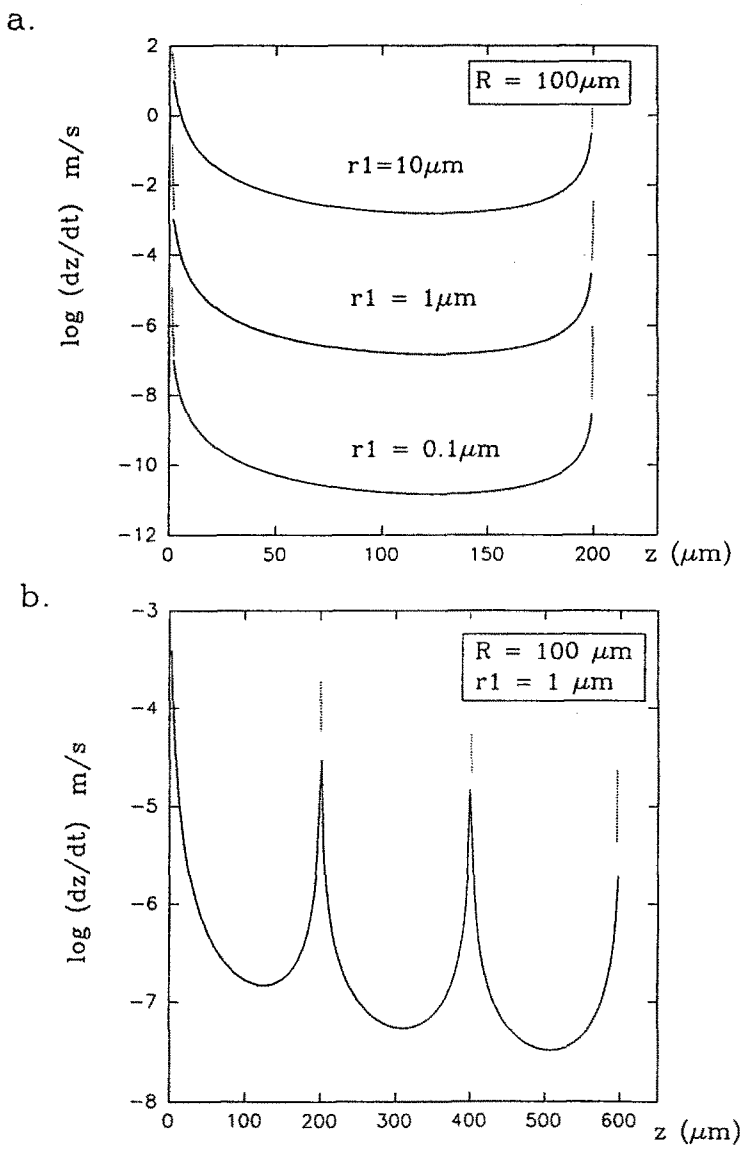

Fig. 4. Imbibition velocity (dz/dt) versus height (z) for spherical element of 100 μm radius. (a) with different access radius. (b) succession of 3 spherical elements with 1 μm access radius.

and the filling kinetics of the entire tube is a smooth curve, fitting as expected, with a square root function (Figure 6b).

In order to simplify the calculation for the filling kinetic over the entire tube, it could be conceivable to calculate it with a cylindrical tube which effective radius (r_{eff}) can be determined from the global imbibition kinetic of the single spherical element. Nevertheless, the result of this procedure does not accord with that of the proposed tube model: for example in a spherical unit with $R = 10\,\mu m$ and $r_1 = 1\,\mu m$, r_{eff} is

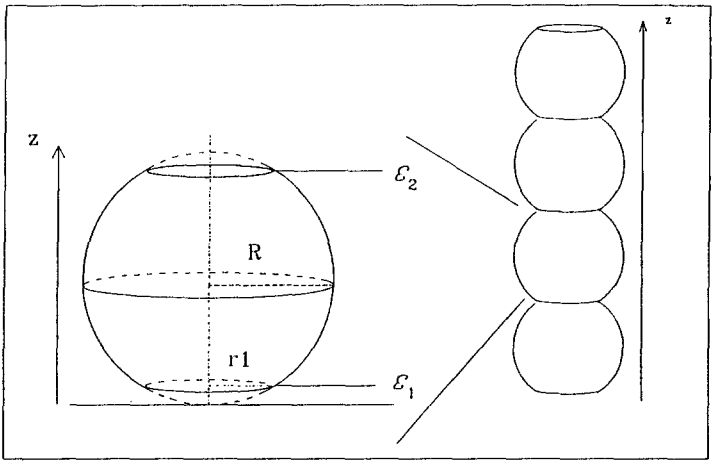

Fig. 5. 'Spherical' element of the model.

1.6×10^{-3} μm, and when calculated over 5 cm, B is 1.85 cm/$\sqrt{h}$ for the proposed tube model, whereas for the cylinder it is 0.87 cm/$\sqrt{h}$. So the model of sphere stack tube requires calculation with Equation (9) and cannot be assimilated to cylindrical tube.

This model provides a kinetic behaviour agreeing with experimental features, so it can be compared with the experimental capillary imbibition kinetics. Two experimental geometrical data are necessary to feed this model: the sphere radius R and the access pore radius r_1.

5. Determination of Model Parameters

Considering only two parameters to describe the pore size and geometry of natural rock is an extreme simplification of its real network. It implies a single pore shape and uniform pore size distribution. However despite this simplification, in many cases one can suppose that only one pore size and geometry regulates the capillary imbibition phenomenon (Dullien *et al.*, 1977). To this end, we tried to determine a single pore radius (R) and single pore access radius (r_1) for natural rocks. Various methods have been tested for the quantification of these two parameters. Mercury intrusion porosimetry for example, provides a pore size distribution in porous media. As this method is based on the introduction of a nonwetting fluid into the porous network, the necks and pore access radii will determine the mercury penetration (Dullien, 1979; Chatzis and Dullien, 1981; Good and Mikhail, 1981). When the pore size distribution is unimodal, a threshold corresponding to the most important pore access radius can be defined graphically (Figure 7) and can be assigned to the r_1 value of the model. On the other hand, in order to determine the pore radius (R), microscopical observation of rock sample thin sections can be used. The thin sections are previously saturated with coloured epoxy resins or a metallic alloy, in

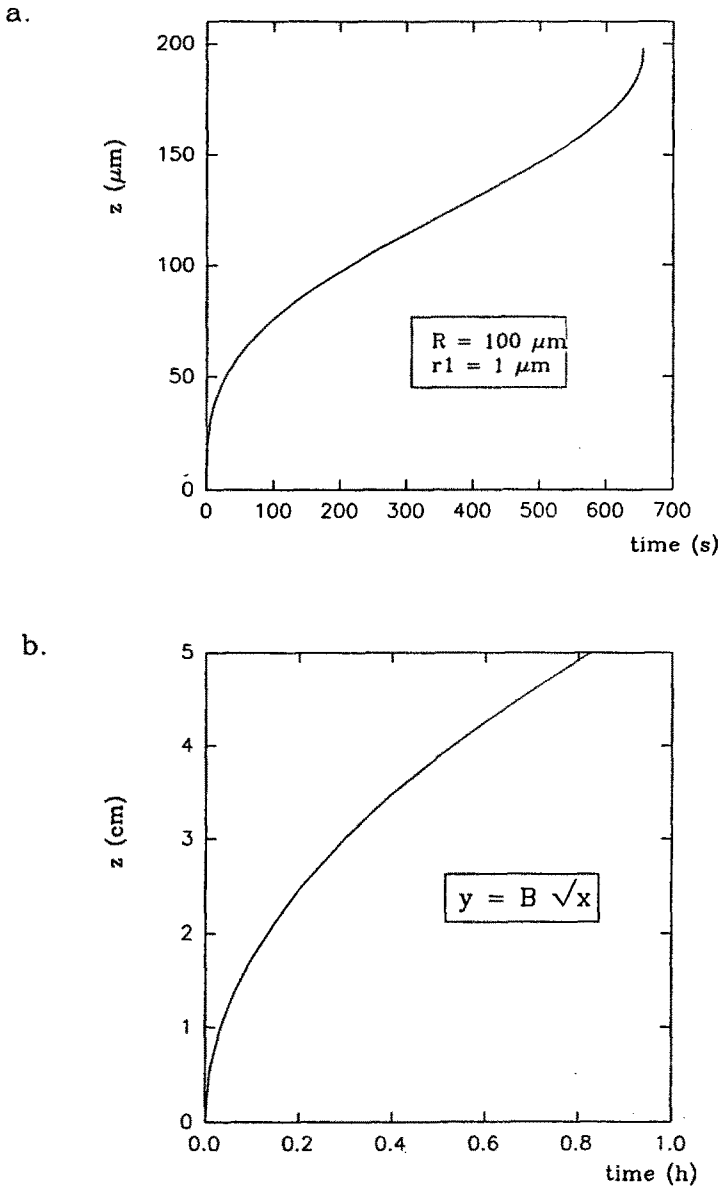

Fig. 6. Capillary imbibition kinetic into (a) a spherical element, (b) into a 5 cm height network, composed by a spherical elements succession.

order to optimize the porous network observation (Dullien, 1981; Zinszner and Meynot, 1982) as shown in Figure 8. Then the pore dimensions and the pore size distribution curve can be measured either directly or indirectly by numerical analysis of the images. Considering the most frequently occurring pore size as representative for the mean pore radius involved in capillary imbibition, R is determined. This method can easily be used for coarse and clayless rocks, but for

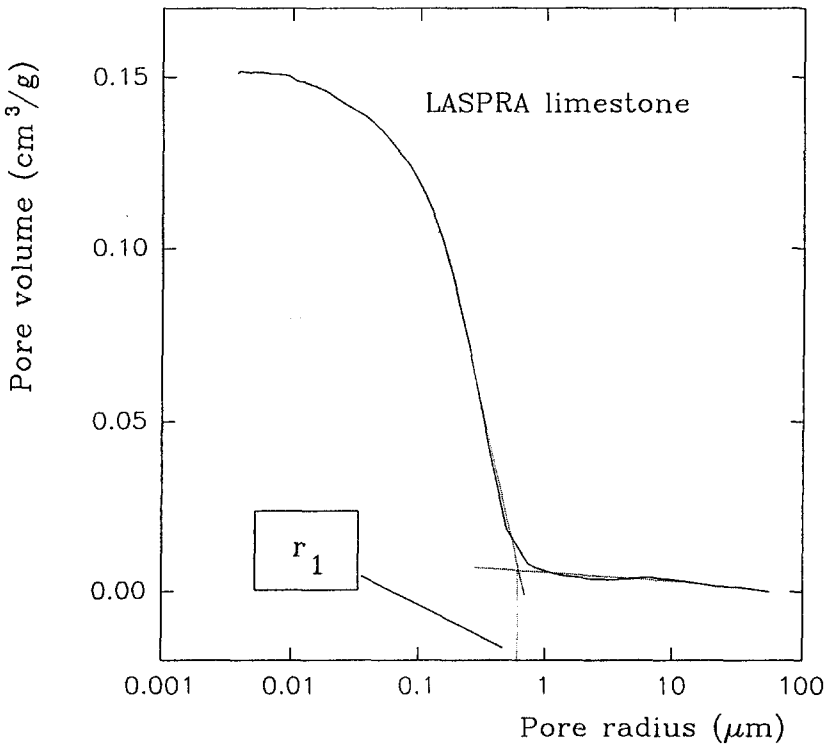

Fig. 7. Average pore access radius r_1 determination on a porosimetry curve.

very fine porous systems (e.g. micritic limestones), microscopical discrimination cannot be used.

In order to estimate this structural parameter for very fine rocks, an alternative method using BET surface area data has been developed. Assuming that sedimentary rocks structures can be described by a solid sphere pack model, a simple relation between particle size and surface area S_t is pointed out for spheres of uniform radius R_s:

$$S_t = 4\pi R_s^2$$

and surface volume rate:

$$\frac{S_t}{V} = \frac{4\pi R_s^2}{4/3\pi R_s^3}.$$

Hence for specific surface area S, calculated with BET equation from nitrogen adsorption isotherms (Lowel and Shields, 1984), this relation becomes:

$$R_s = \frac{3}{\rho S}, \tag{10}$$

where ρ is the true rock density. Using the particle size calculated with the specific surface area measurement, the pore radius R and pore access radius r_1 can be

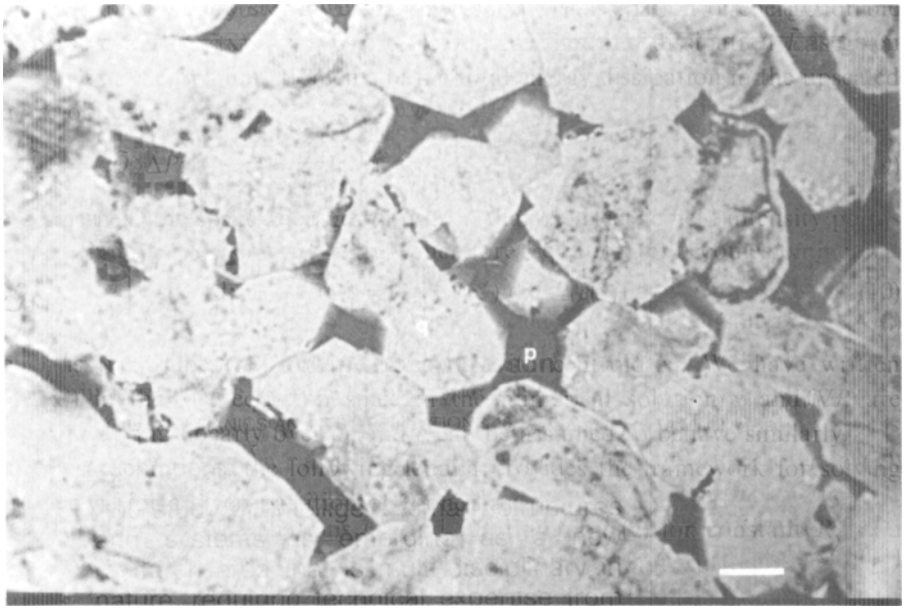

Fig. 8. Micrograph of Fontainebleau sandstone thin section. **p**: pore, **q**: quartz (reference mark: 100 μm).

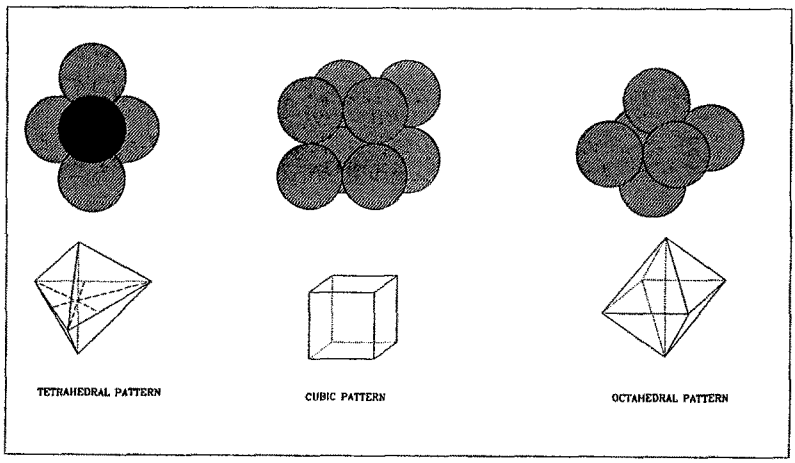

Fig. 9. Three sphere packing patterns.

Table I. Pore radii for various packing patterns

Packing pattern	R	r_1
Cubic	$R_s/\sqrt{2}$	$R_s(\sqrt{8}-2)/2$
Tetrahedral	$R_s\sqrt{(2\sqrt{3}-\pi)/2\pi}$	$R_s(2\sqrt{3}-3)/3$
Octahedral	$R_s(\sqrt{8}-2)/2$	$R_s(2\sqrt{3}-3)/3$

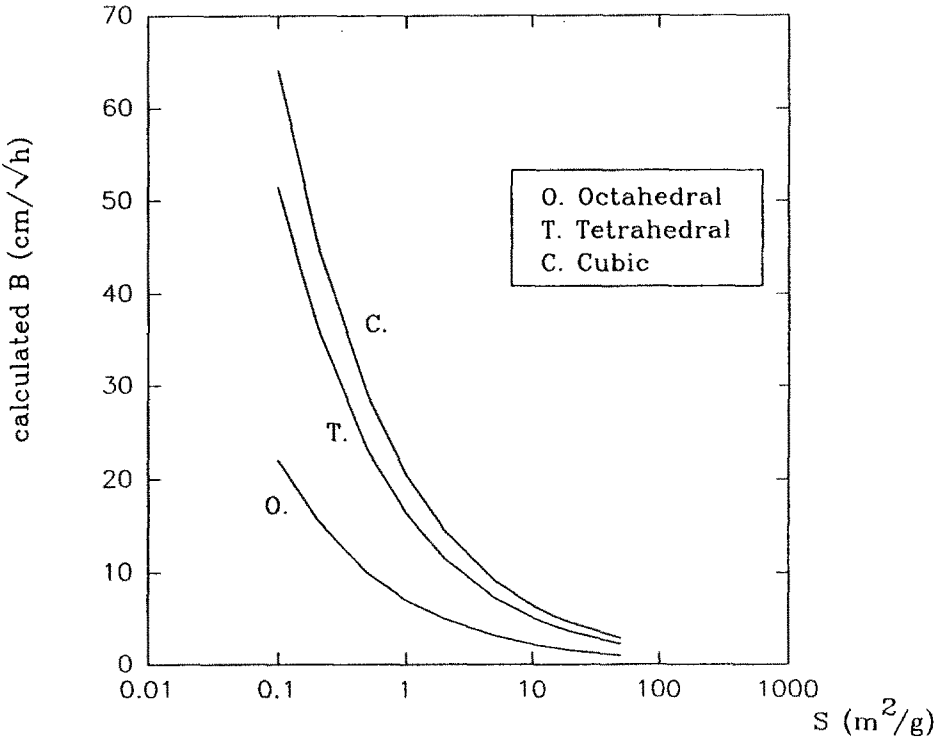

Fig. 10. Capillary rise kinetic (B) versus specific surface area (S) for the three sphere packing patterns.

deduced for various packing models. On the basis of cubic, tetrahedral and octahedral packing patterns (Figure 9), R and r_1 have been determined in relation to the particle radius R_s (Table I). Next, a direct relation between specific surface area and capillary kinetics is derived for each packing pattern, as shown in Figure 10. As radii, and especially pore access radius r_1, decrease with increasing specific surface area S, the capillary rise kinetics (B) decreases with increasing specific surface area (S). The various packing models lead to large differences for capillary imbibition kinetics, and particularly for low specific surface areas.

6. Practical Application and Discussion

In order to test this model with natural rocks, it was applied to some Spanish and French sedimentary rocks:

- Laspra micritic magnesian limestone,
- Hontria bioclastic limestone,
- Lourdines micritic limestone,
- Fontainebleau sandstone.

Some of their petrographical and physical characteristics are shown in Table II. These four rock types present a wide range of texture, mineralogy and capillary

Table II. Petrographical and physical characteristics of the four rock types. N_I: free porosity; B: experimental average capillary rise kinetics ± standard deviation; S: specific surface area

Rock type	Mineralogy	Texture	N_I (%)	B cm/$\sqrt{h}$	S m²/g
Laspra limestone	dolomite 90% quartz 10%	very fine	28	2.39 ±20%	4.6
Hontoria limestone	calcite 99% quartz 1%	coarse	18	7.1 ±12%	0.8
Lourdines limestone	calcite >99%	fine	22.8	5.5 ±7%	1.65
Fontainebleau sandstone	quartz >99%	coarse	4.8	10.3 ±15%	0.4

Table III. Pore radii R, pore access radii r_1 and calculated imbibition kinetic parameter B for the four rock types and the three packing patterns. C: cubic, T: tetrahedral, O: octahedral

Rock type		R μm	r_1 μm	$B_{calc.}$ cm/$\sqrt{h}$
Laspra	C	0.17	0.1	8.08
	T	0.05	0.04	6.40
	O	0.1	0.04	2.76
Hontoria	C	1.02	0.57	19.65
	T	0.31	0.21	15.60
	O	0.57	0.21	6.76
Lourdines	C	0.49	0.28	13.73
	T	0.15	0.10	10.91
	O	0.28	0.10	4.70
Fontainebleau	C	2.07	1.17	28.13
	T	0.64	0.44	22.33
	O	1.17	0.44	9.65

imbibition kinetics parameters, and makes them suitable to check the model. Using Equation (10) and the relations in Table I, the pore and pore access radii were calculated (Table III). Then, on the basis of Equation (9), imbibition kinetics parameters were calculated for all the rock types and for the three packing geometries. The results for capillary rise kinetics (B) were plotted against experimental B kinetics (Figure 11). For each rock type, tetrahedral and cubic packing patterns provide kinetic values two and three times higher than experimental data. So these two packing geometries appear to be inappropriate. The B values calculated from the octahedral packing geometry, agree very well with the experimental results. The maximum deviation of calculated B values from experimental ones, is about 15%. The experimental error on B ranged from 7 to 20%.

Despite the fact that this model provides good results, two points have to be interpreted. First, if octahedral packing geometry is valid, then there should be a

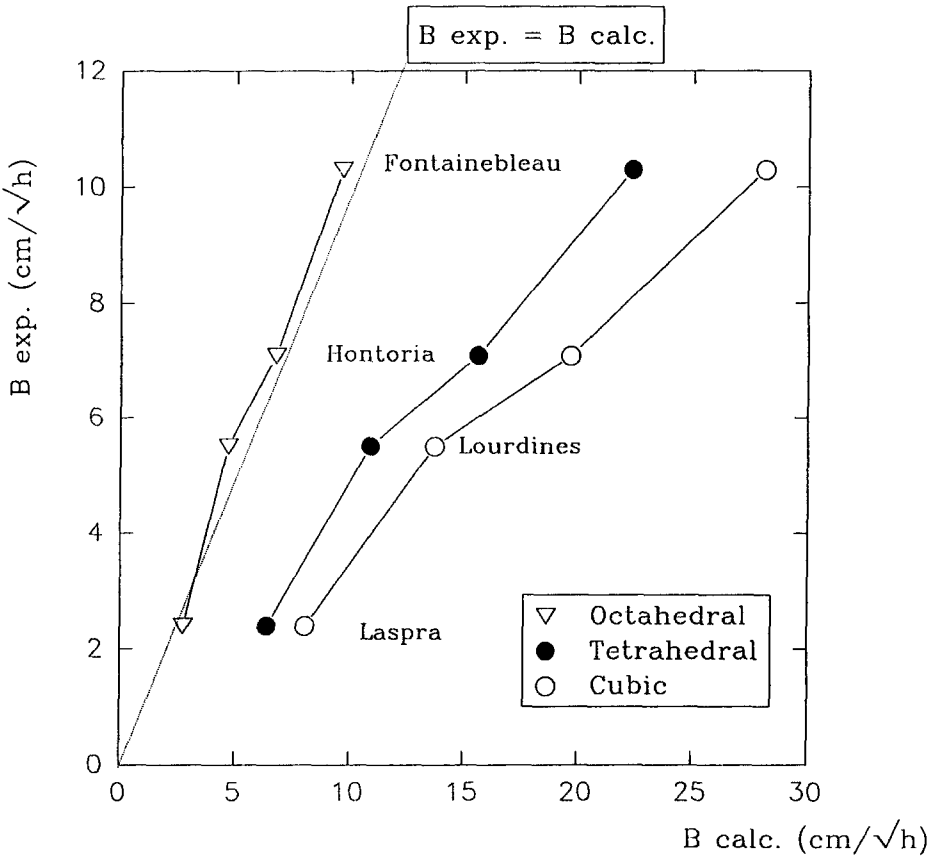

Fig. 11. Experimental B values versus calculated B values for the four rock types and the three packing patterns.

constant ratio between pore radius R and pore access radius r_1 ($R/r_1 \approx 2.677$), and the porosity should be the constant ($\approx 27.8\%$) independent of rock types. Obviously observed porosities are not similar, at least at a macroscopical scale. On the other hand, the specific surface area for Fontainebleau sandstone for example (0.8 m^2/g) does not agree with the sizes of its grains (200–400 μm) shown in Figure 8.

The only way to explain these features is by taking into account surface roughness. Dullien *et al.* (1989) showed that it can be considered as a microscopical porous network developed on the surface of the macroscopical grains, strongly modifying the capillary imbibition. Hydrodynamical and specific surface area arguments tend to confirm its presence and it may be assumed that its porosity and dimensions conform with those of the model.

The specific surface area seems to be a good parameter to determine pore dimensions for capillary imbibition. Nevertheless, this condition is not sufficient, it is also necessary to chose an appropriate pore shape. White (1982) for example

Table IV. Experimental and calculated B values. B_W: after White (1982) model. B: after proposed model

Rock type	B_{exp}	B_W	B
Laspra	2.39	9.18	2.76
Hontoria	7.1	17.15	6.76
Lourdines	5.5	14.87	4.7
Fontainebleau	10.3	17.045	9.65

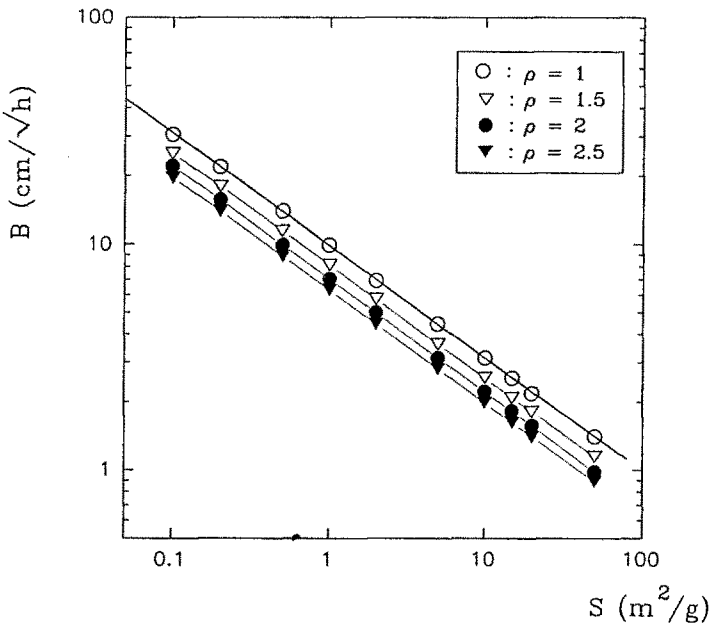

Fig. 12. B versus specific surface area S for different true density values. Solid line: empirical equation $B = 9.882/S^{0.497}$ for true density $\rho = 1$.

suggested a formula for cylindrical tubes involving specific surface area (S) and porosity N to determine an effective radius r_{eff}.

$$\left.\begin{aligned} A/V &= 2/r_{eff} \\ A/V &= (1-N)S/N \end{aligned}\right\} r_{eff} = \frac{2N}{(1-N)S}.$$

By introducing this radius value in Washburn's equation for cylindrical tube, B has been calculated for the four rock types. The results shown in Table IV are less satisfactory than those of the first model.

The direct implication of the proposed model is that a single specific surface area measurement for these sedimentary rocks, enables the determination of their behaviour for capillary imbibition kinetics. So an empirical function could be determined between specific surface area (S) and capillary rise kinetics (B) for true density = 1 (g cm^{-3}):

$$B = \frac{9.882}{S^{0.497}}. \tag{11}$$

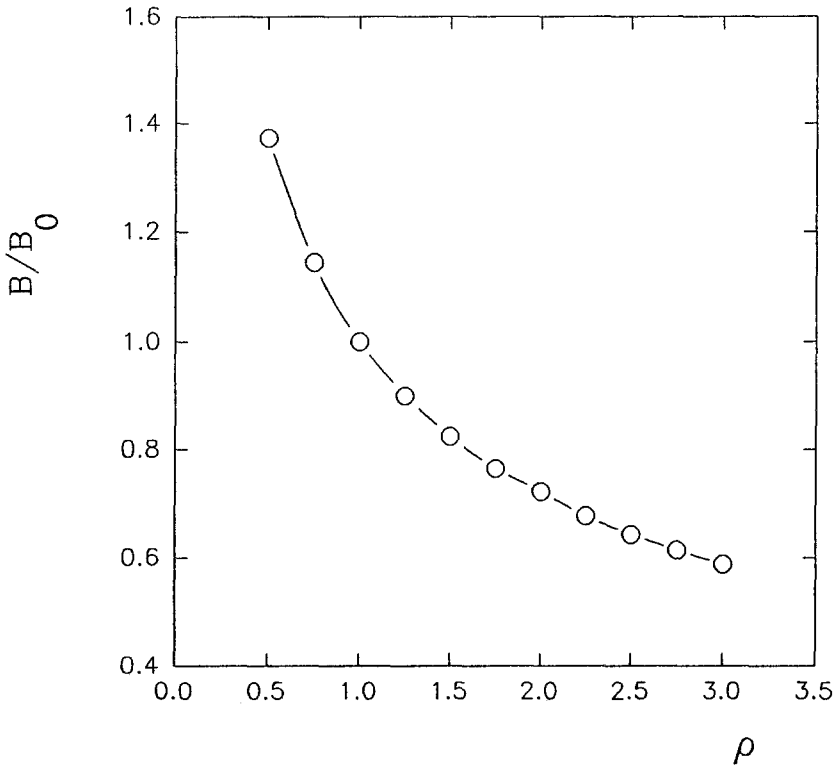

Fig. 13. Relative rising damp migration kinetic B/B_0 versus true density ρ.

As shown in Figure 12, $B = f(S)$ relations are proportional for each density value. With this representation, $B = f(S)$ fits as $\log(B) = a\log(S) + b$, where a keeps constant and b density dependant. Hence calculating B_0 (B for $\rho = 1$) with the empirical Equation (10), B can be settled for any density value as represented in Figure 13. Moreover, as this relation is direct between S and B, it could also be applied conversely, because by knowing the capillary imbibition kinetics parameters and the true rock density, it should be possible to estimate the specific surface areas for such rock types, using this model.

7. Conclusion

A tube model built with a periodical succession of hollow spheres has been elaborated, in order to simulate capillary imbibition kinetics in porous sedimentary rocks. The proposed pore shape allows simple mathematical iterative computer processing using experimental pore size data. Two parameters are necessary to feed this program: average pore radius R and average pore aceess radius r_1. The best method to obtain these parameters, is considering spherical uniform particles, whose radius can be calculated from specific surface area data, and further the pores radii are determined by applying sphere packing models. Octahedral packing geometry

gives good agreement with the experimental B values for four different sedimentary rock types. For Fontainebleau sandstone it has been pointed out that specific surface area and capillary imbibition appears to be determined by surface roughness.

As only octahedral packing provides suitable results for all rock types, a direct relation between specific surface area and capillary imbibition kinetics relation can be derived. So a single specific surface area measurement allows prediction of capillary imbibition kinetics, and conversely with experimental capillary, specific surface area can be determined.

Acknowledgements

We would like to thank Dr Jose B. Parra Soto of Instituto Nacional del Carbon de Oviedo (Spain) and Dr Jean Eric Poirier of U.A. 235, Minéralurgie, University of Nancy (France) for specific surface area measurements on rock samples. The senior author also acknowledges Dra Rosa M. Esbert of the Department of Geology of the University of Oviedo (Spain) for her welcome in her section and her assistance with rock sampling and characterization.

References

Chatzis, I., and Dullien, F. A. L., 1981, Mercury porosimetry curves of sandstones. Mechanisms of mercury penetration and withdrawal, *Powder Technol.* **29**, 117–125.

Dullien, F. A. L., El-Sayed, M. S., and Batra, V. K., 1977, Rate of capillary rise in porous media with nonuniform pores, *J. Colloid Interface Sci.* **60**, 497–506.

Dullien, F. A. L., 1979, *Porous Media: Fluid Transport and Pore Structure*, Academic Press, New York, pp. 291–300.

Dullien, F. A. L., 1981, Wood's metal porosimetry and it's relation to mercury porosimetry, *Powder Technol.* **29**, 109–116.

Dullien, F. A. L., Zarcone, C., Macdonald, I. F., Collins, A., and Bochard, R. D. E., 1989, The effect of surface roughness on the capillary pressure curves and the height of capillary rise in glass bead packs, *J. Colloid Interface Sci.* **127**, 362–372.

Good, R. J. and Mikhail, R. S., 1981, The contact angle in mercury intrusion porosimetry, *Powder Technol.* **29**, 53–62.

Kusakov, M. M. and Nekrasov, D. N., Capillary hysteresis in the rise of wetting liquids in single capillaries and porous bodies, in Deryagin, B. V., 1966, *Research in surface forces*, New-York, pp. 193–202.

Levine, S., Lowndes, J., and Reed, P., 1980, Two phase fluid flow and hysteresis in a periodic capillary tube, *J. Colloid Interface Sci.* **77**, 253–263.

Lowel, S. and Shields, J. E., 1984, *Powder surface area and porosity*, Chapman and Hall, London, pp. 1–5.

Marmur, A., 1989, Capillary rise and hysteresis in periodic porous media, *J. Colloid Interface Sci.* **129**, 278–285.

Mertz, J. D., 1989, *Rôle des structures de porosité dans les propriétés de transport*, thèse Université Louis Pasteur, Strasbourg.

Szekely, J., Neumann, A. W., and Chuang, Y. K., 1971, The rate of capillary penetration and the applicability of the Washburn equation, *J. Colloid Interface Sci.* **35**, 273–283.

Van Brakel, J., Pore space models for transport phenomena in porous media. Review and evaluation with special emphasis on capillary transport, *Powder Technol.* **11**, 205–236.

Washburn, E. W., 1921, The dynamic of capillary flow, *Phys. Rev.* **17**, 273–283.

White, L. R., 1982, *J. Colloid Interface Sci.* **90**, 536– .

Zinszner, B. and Meynot, C., 1982, Visualisation des propriétés capillaires des roches reservoirs, *Rev. Inst. Franç. du Pétrole* **37**, 337–361.